SOLPS-ITER Modeling of the Alcator C-Mod Divertor Plasma*)

Wouter DEKEYSER, Xavier BONNIN, Steven W. LISGO, Richard A. PITTS, Dan BRUNNER[1)], Brian LABOMBARD[1)] and Jim L. TERRY[1)]

ITER Organization, Route de Vinon-sur-Verdon, CS 90 046, 13067 St Paul Lez Durance, France
[1)]*MIT Plasma Science and Fusion Center, Cambridge, MA 02139, USA*

(Received 1 April 2016 / Accepted 25 May 2016)

SOLPS-ITER is a new edge code package that will be developed and maintained at the ITER Organization [X. Bonnin *et al.*, Plasma Fusion Res. **11**, 1403102 (2016)], in close collaboration with the wider SOLPS community, and will be used to support the design of the ITER divertor [A.S. Kukushkin *et al.*, Fusion Eng. Des. **86**, 2865 (2011)]. In this paper, we report on the first application of the code to the modeling of the Alcator C-Mod divertor. With its high density, high magnetic field, and strong ITER-like target shaping, C-Mod is of particular interest to ITER in terms of plasma and neutral parameters in the divertor. We show that with a fluid neutral model, we can qualitatively reproduce the observed particle fluxes to inner and outer targets under partially detached conditions. However, simulated electron temperatures in the divertor are much too low. A number of physics and numerical reasons are proposed to resolve this issue and serve as a guideline for further development of the code.

Keywords: edge plasma modeling, divertor modeling, scrape-off layer, SOLPS-ITER, Alcator C-Mod

DOI: 10.1585/pfr.11.1403103

1. Introduction

The SOLPS-ITER code [1] is a new plasma boundary modeling package developed and hosted at the ITER Organization, and is a backward-compatible successor to the SOLPS4.3 code, which was used to guide the design of the ITER divertor [2]. It is based on the most recent, MPI-parallelized version of the kinetic neutral particle transport code Eirene, and the B2.5 plasma code version developed in St. Petersburg, which presently includes the most advanced numerical treatment of drifts and currents [3].

In order to improve the predictive capabilities of the code and to identify and study remaining modeling issues, it is essential that the edge plasma model in SOLPS-ITER be continuously validated against other edge codes and experimental data from existing devices. As a part of this effort, we initiated a benchmarking study by modeling the Alcator C-Mod divertor plasma. With its magnetic field, divertor density and target shaping very close to ITER design values, the C-Mod divertor is one of the most ITER-relevant experiments in terms of divertor plasma and neutral particle parameters.

To date, most plasma edge code studies of Alcator C-Mod have been performed with the UEDGE code, focussing on the development of fluid neutral models [4] and on modeling the strong Main Chamber (MC) recycling regime found on C-Mod [5]. Early studies with the B2-Eirene code include [6], where the so-called 'death ray' phenomenon found experimentally near detachment was investigated. This was later found to be an artifact associated with operating a Langmuir probe under conditions of very high density and high neutral pressures [7, 8]. More recent numerical studies of the C-Mod edge plasma with SOLPS5.0 focused mainly on the numerical stability of the code in neutral dominated regimes [9], and on the study of fluid drifts in the context of explaining the strong experimentally observed scrape-off layer (SOL) flows [10, 11]. To our knowledge, there have been no further SOLPS studies of the C-Mod divertor. It has, however, previously been modeled extensively with the OSM-Eirene code suite [12], in which the divertor plasma solution has been reconstructed using an Onion-Skin Method, using experimental data as input. The focus of the work was on matching experimentally measured neutral pressures in the sub-divertor volumes by studying the impact of different processes in the kinetic neutral transport model.

In this paper, we report on the first results of the application of the new SOLPS-ITER package to modeling of the C-Mod divertor. The paper is organized as follows: in Sec. 2, the C-Mod discharge chosen for this initial benchmark is introduced. Section 3 briefly discusses the SOLPS-ITER edge plasma model and the modeling details for our benchmark study. Results are presented in Sec. 4. Finally, conclusions and future work are discussed in Sec. 5.

2. Experiment

As an initial benchmark for the new code, the deuterium, ohmic discharge number 990429019 at 950 ms has

author's e-mail: wouter.dekeyser@iter.org

*) This article is from 15th International Workshop on Plasma Edge Theory in Fusion Devices.

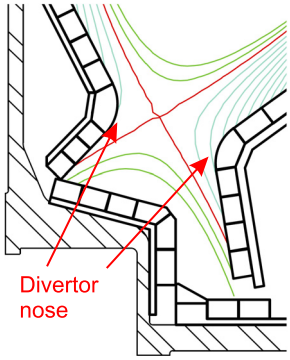

Fig. 1 Cross section of the old C-Mod divertor (1999).

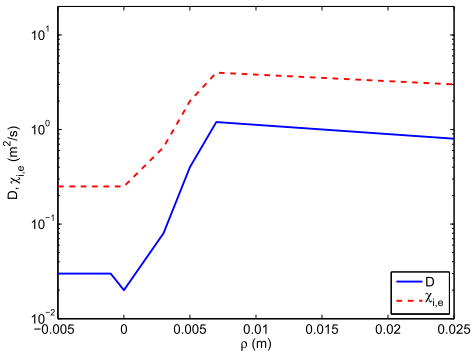

Fig. 2 Radial profiles for anomalous transport coefficients.

been chosen. This plasma pulse has $I_p = 0.8\,\mathrm{MA}$, $B_T = 5.4\,\mathrm{T}$, and a line average density of $\bar{n}_e = 1.46 \times 10^{20}\,\mathrm{m}^{-3}$. This is considered a medium-density discharge on C-Mod. The magnetic geometry is single-null, with lower X-point, and the ion $B \times \nabla B$ drift direction pointing down. This same shot was also used to model divertor neutral pressures in [12]. A cross section of the C-Mod divertor at the time of the shot is shown in Fig. 1.

The ohmic power obtained from an EFIT-reconstruction is $P_{OH} \sim 1\,\mathrm{MW}$, and radiated power in the core measured with a diode detector is estimated at $P_{rad} \sim 500\,\mathrm{kW}$, fairly high for this type of discharge. Outer midplane profiles of electron density and temperature obtained with a Horizontal Scanning Probe (HSP) are shown in Fig. 3. Target data for ion saturation current and electron temperature are obtained from Langmuir probes (LP) embedded in the target plates (Fig. 4). Within the caveats associated with the interpretation of Langmuir probes in cold magnetized plasmas (see Sec. 4), the measurements show a partially detached inner target and an outer target in the high recycling regime, which is close to the divertor operating regime presently foreseen on ITER [2], where both targets are partially detached. Even for this ohmic discharge, the peak ion flux to the outer target is only a factor ~ 3 lower than the target value foreseen in the ITER baseline scenario [13].

3. Modeling with SOLPS-ITER

The edge plasma solver in SOLPS-ITER consists of a coupling between a multi-fluid, finite-volume code for the ions and electrons, B2.5, and the kinetic neutral transport code Eirene. B2.5 solves a set of continuity and parallel momentum equations for each ion species, and energy equations for the ion temperature T_i and electron temperature T_e. Furthermore, the electric potential ϕ is deduced from the current continuity equation, $\nabla \cdot \mathbf{j} = 0$. Parallel transport is based on the Braginskii equations, while radial transport is modeled through the specification of anomalous diffusion coefficients, viscosities and heat conductivities. B2.5 also has a fluid neutral model available for atomic species, solving a separate continuity and parallel momentum equation for each neutral species and assuming a common ion-neutral temperature [14].

Eirene solves a (set of) linear transport equation(s) for neutral atoms and molecules, treating in detail a wide range of collisional processes. Furthermore, a non-linear BGK model for neutral-neutral (atom-atom, atom-molecule and molecule-molecule) collisions is available [15].

For this initial code study, we assume a single fluid, Deuterium plasma, and use the fluid neutral approximation on the B2.5 side. The plasma model equations and numerical implementation according to SOLPS5.2 [16] are used, including the correct treatment of the vectorial nature of the parallel momentum equation and the centrifugal force. Drift terms are not included at this stage of the study.

3.1 Anomalous radial transport

Since divertor conditions are extremely sensitive to upstream separatrix conditions, it is important to match the upstream conditions well in the simulation. Radial transport coefficients have been tuned to match outer midplane profiles of electron density and temperature. The resulting profiles of the radial diffusion coefficient D and the electron and ion heat conductivities χ_e and χ_i are shown in Fig. 2 as a function of ρ, the distance from the separatrix as measured at the outer midplane. Since there is no experimental data on the ion temperature for this shot, we assume $\chi_i = \chi_e$ in the simulations. We note a strong increase of D towards the far SOL, by almost two orders of magnitude compared with the value at the separatrix. Similar trends and absolute values have been inferred from experimental data [5]. There are no experimental profiles for χ_i or χ_e available, but the strong radial increase is in line with detailed edge plasma modelling in ASDEX-Upgrade [17,18].

3.2 Boundary conditions

At the core boundary of the modeling grid, the input power is $P_{OH} - P_{rad} \sim 500\,\mathrm{kW}$, divided equally between ions and electrons. Even though the line average density slowly increases during the reference plasma shot, we assume steady-state on the time scales relevant to the SOL.

There is no central fuelling in C-Mod, so we have a zero mass flux boundary condition at the inner boundary. For the fluid neutral model, we translate the zero mass flux condition at the core to zero flux for both ions and neutrals. Since there was no pumping during the discharge and we can assume the wall was fully saturated at 950 ms into the shot, we set the recycling coefficients for the neutrals uniformly to 1.00 at the divertor targets, and at the private flux region (PFR) and main chamber (MC) boundaries. As a result, within the accuracy of the time integration scheme of the code, the particle content in the simulation is fully determined by the value for the initial plasma state. A 'density scan' can therefore be performed by simply scaling the initial particle content of the plasma.

At the targets, sheath conditions are applied. Plasma sound speed c_s is imposed for the parallel velocity ($M = 1$), while poloidal ion and electron internal energy fluxes $q_{x,i}$ and $q_{x,e}$ are fixed using transmission coefficients $\gamma_i = 1.5$, $\gamma_e = 1 + \frac{e\phi}{T_e}$, and the potential ϕ computed self-consistently from the boundary condition for the poloidal current j_x:

$$q_{x,i} = \gamma_i n_i b_x c_s T_i,\ q_{x,e} = \gamma_e \left(n_e b_x c_s - \frac{j_x}{e} \right) T_e,$$

$$j_x = e n_e b_x \left(c_s - \frac{1}{\sqrt{2\pi}} \sqrt{\frac{T_e}{m_e}} \exp\left(-\frac{e\phi}{T_e} \right) \right), \qquad (1)$$

where b_x is the magnetic field pitch, $c_s = \sqrt{\frac{T_i + T_e}{m_i}}$ the plasma sound speed, and e the unit of charge. All temperatures are in units of Joules.

Since extended grids, which allow for boundary plasma simulations all the way up to the main chamber wall [19], are presently not available in SOLPS-ITER, the ion and internal energy fluxes to the MC and PFR boundaries are specified through leakage boundary conditions of the form:

$$-D \frac{1}{h_n} \frac{\partial n_i}{\partial n} = \delta_{n_i} n_i c_s, \qquad -\kappa_i \frac{1}{h_n} \frac{\partial T_i}{\partial n} = \delta_{T_i} n_i c_s T_i,$$

$$-\kappa_e \frac{1}{h_n} \frac{\partial T_e}{\partial n} = \delta_{T_e} n_e c_e T_e, \qquad (2)$$

with $\kappa_i = \chi_i n_i$, $\kappa_e = \chi_e n_e$, and $c_e = \sqrt{\frac{T_e}{m_e}}$. Variable n denotes the outward normal direction, and h_n the metric coefficient in this direction. For the results presented below, we use $\delta_{n_i} = 1.25 \cdot 10^{-3}$, $\delta_{T_i} = 1 \cdot 10^{-2}$, and $\delta_{T_e} = 1 \cdot 10^{-4}$. These leakage conditions are similar in nature to decay length conditions. At any particular position, a leakage factor δ_{n_i} implies an equivalent decay length of $\lambda_{n_i} = \frac{D}{\delta_{n_i} c_s}$. Equivalent expressions apply for the ion and electron temperature decay lengths. However, since c_s and c_e vary poloidally at the MC and PFR boundaries, the equivalent decay lengths also vary with poloidal location along the boundaries. We note that since these leakage (and decay-length) boundary conditions for continuity and energy equations influence the amount of particles and energy flowing through radial boundaries, they also indirectly determine the steepness of the density and temperature profiles for a given set of transport coefficients. Therefore, the radial boundary conditions cannot be tuned independently of the radial profiles of the anomalous transport coefficients, and finding a good match to all experimental profiles critically depends on finding a consistent parameter set. In this respect, the introduction of extended grids will be a big step forward in at least partially removing the uncertainty in boundary conditions by replacing leakage or decay-length type boundary conditions with more standard sheath conditions at the true MC and PFR vessel boundaries.

4. Modeling Results

The midplane electron density and temperature profiles simulated with SOLPS-ITER are compared to the HSP data in Fig. 3. The results of three simulations are shown: a reference case labelled 'SOLPS-ITER', and two other cases with 30% lower and 25% higher particle content, labelled 'SOLPS-ITER, ×0.70' and 'SOLPS-ITER, ×1.25', respectively. These cases will be referred to as 'reference', 'low density' and 'high density' cases below. The same radial transport coefficients and boundary conditions have been used for all three cases. We note very good qualitative and quantitative agreement with the upstream experimental data. Both the separatrix values and the far-SOL values of electron density and temperature are matched well in the reference case. The simulated ion temperature profiles are also shown on the right in Fig. 3. Since we have used the same profiles for radial ion and electron heat conductivities and similar leakage boundary conditions, the resulting ion temperature is quite close to the electron temperature. For almost the entire domain, we have $0.7 \leq T_i/T_e \leq 1.5$. More recent studies of the ion temperature on C-Mod have shown ratios of $T_i/T_e \sim 2$ along the separatrix for conditions near detachment [20], but in the absence of data for the specific discharge modeled here, we have only ensured $T_i \gtrsim T_e$ thus far. The effect of the temperature ratio on divertor conditions will be subject of future work.

The three simulated cases show quite different behavior at the inner and outer targets. Figure 4 shows simulated profiles of ion saturation current (j_{sat}), electron temperature and electron density compared to Langmuir probe data, mapped to the outer midplane. The experimental data shows an outer target which is clearly attached, with ion saturation current and electron pressure peaked at the strike-point. In the simulation, the peak value of the ion saturation current is matched quite well for the reference case and the low density case: values of $1.2\,\mathrm{MA\,m^{-2}}$ in the simulations compared to $1.3\,\mathrm{MA\,m^{-2}}$ measured experimentally. However, the peak occurs slightly outside the strike-point in the model and the radial decay (positive ρ) is less steep, giving profiles that are too broad. In the high density case, the ion saturation current and pressure at the

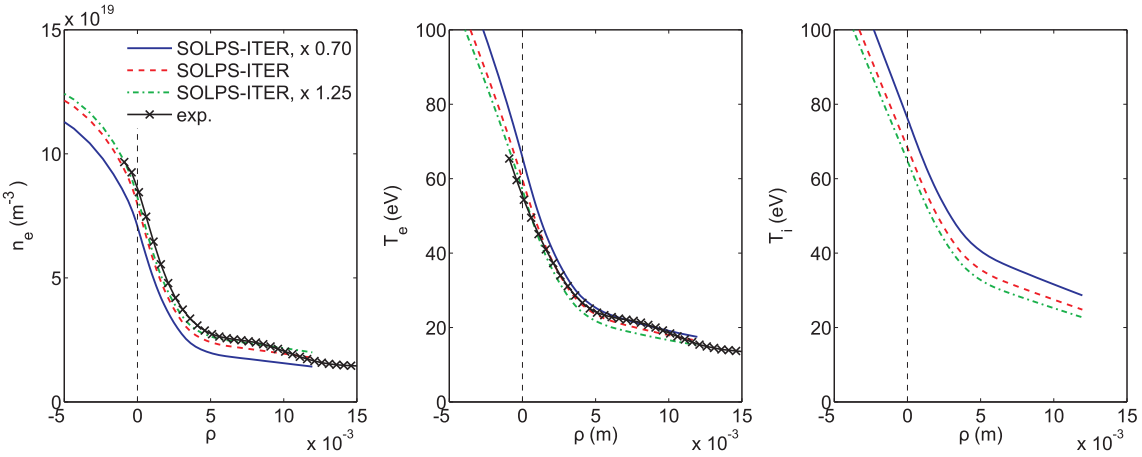

Fig. 3 Upstream profiles of electron density (left), electron temperature (centre), and ion temperature (right).

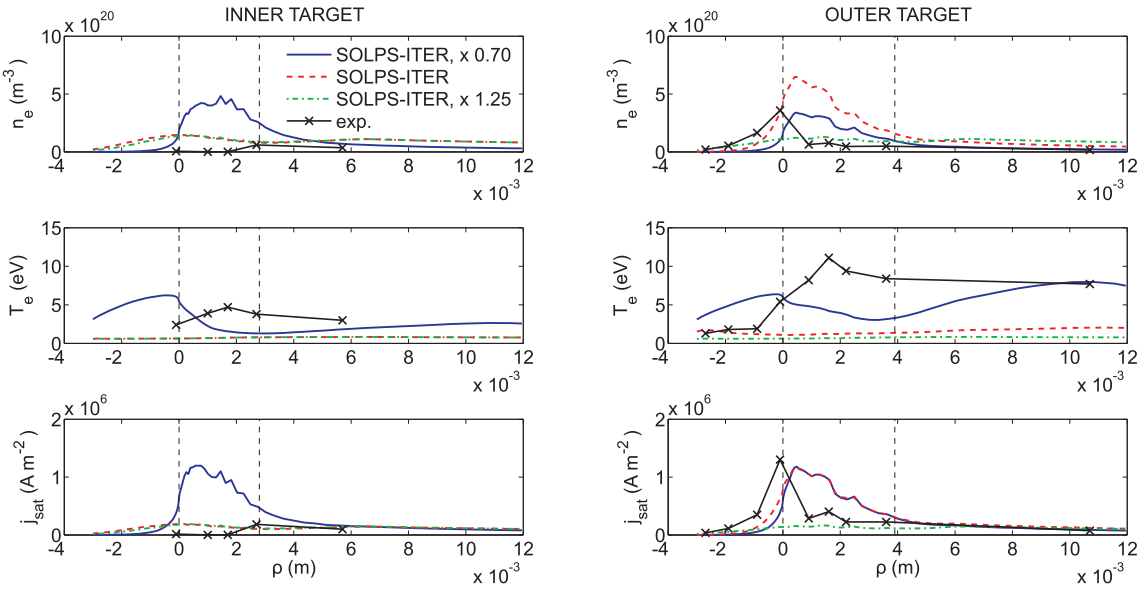

Fig. 4 Target profiles of electron density (top), electron temperature (middle), and ion saturation current (bottom). Left: inner target, right: outer target.

outer target have dropped to very low values, indicating detachment in the simulation.

At the inner target, the experimental ion saturation current data, as well as a comparison of upstream to target electron pressures, show clear detachment in the first few millimeters outside the strike-point (when mapping to the outer midplane), and possibly reattachment at the divertor nose (see Fig. 1, indicated with a vertical dashed line at ~ 3 mm in Fig. 4). However, spectroscopy data (not shown here) shows that the probe T_e values are too high above the nose, and the plasma is likely still detached there [12]. In the simulations, we also observe detachment for the reference and high density cases. Further analysis shows an ionization front moving towards the X-point and a zone of cold plasma where strong volume recombination takes place developing in front of the inner target, which suppresses the ion saturation current at the plate.

The measured electron temperatures at the outer target suggest high recycling conditions at this target, but probably (near) detached conditions in the PFR. T_e is a fitted quantity in the measurement, but with the fairly high ion fluxes in the high recycling regime this measurement is generally considered quite reliable. On the other hand, with values slightly above 1 eV along the entire outer target, the simulated electron temperature in the reference case is much too low compared to experiment, showing that in the simulation the target is in very high recycling conditions or close to detachment. In the high density case, the temperature has dropped below 1 eV and strong volume recombination in front of the target has also eliminated the

ion saturation current. Only if we strongly reduce the particle content in the scan does the simulated target temperature increase again (low density case in the figures). In this case the upstream separatrix density (temperature) is approximately 15% too low (high) compared to measurement. Even if such low density conditions could in principle be achieved by fairly small displacements of the upstream measured profiles (less than 1 mm), the inner target also reattaches and the in-out asymmetry in terms of particle flux is lost.

The experimentally measured electron temperature at the inner target is again much higher than the simulated value. However, in detached conditions temperatures below 1 eV are expected in order to achieve the conditions for strong volume recombination, and temperatures derived from Langmuir probe data under these conditions are known to be questionable [21]. In this respect, the low simulated T_e close to the strike-point is in agreement with that expected for detached conditions.

The experimentally measured n_e is a quantity derived from j_{sat} and T_e. For the high recycling conditions at the outer target the measurements can generally be considered reliable. Also the low density and reference simulations show peaks in electron density at the outer target within a factor 2 of the experimentally measured values, but a profile that is too broad compared to experiment. If the experimentally measured temperature close to the inner target strike-point is questioned, then also the measured density is uncertain. However, both simulation and experiment show low densities as expected in detached conditions.

In this initial study, we can qualitatively reproduce the asymmetry in particle fluxes to the targets, but the simulated outer target temperatures are much too low. There are several reasons why this might be so. The problem could be in the simplified fluid neutral model. However, since the density and therefore the collisionality in the C-Mod divertor plasma are high, a fluid neutral model is expected to be a reasonable approximation. The absence of drifts in the present simulations could also be responsible. Due to its high magnetic field and compact size, drifts are known to be important in C-Mod [10], and could potentially restore the in-out asymmetry in the low density case by redistributing the fluxes of particles and power into the divertor and/or between targets. Filamentary transport in the PFR [22] could also significantly impact the divertor solution. It is also possible that a numerical issue could partially explain the discrepancies. The B2.5 code assumes the grid is perfectly orthogonal, with two faces of each cell aligned with the magnetic field and two faces orthogonal to the poloidal projection of the field. Due to the strongly tilted targets on C-Mod, the actual grid provided to the code is strongly distorted. This has a particularly strong impact on the fluid neutral solution, as discussed in [23]. Indeed, the fluid neutrals tend to migrate toward the far-SOL side of the target, creating an artificially enhanced neutral cushion in that region. This can be eliminated either by implementing a nine-point discretization stencil as in [23], which correctly takes into account grid non-orthogonality, or by using extended grids [19], where the present constraint of topologically rectangular plasma grids on the B2.5 side is relaxed, allowing for orthogonal grids cells up to the target and main-chamber boundaries. Initial observations from a simulation of this C-Mod case with Eirene (which is not affected by grid non-orthogonality) show that indeed the plasma temperature increases away from the strike-points at both inner and outer targets when the fluid neutral model is replaced by Eirene. The impact on the strike-point conditions for this discharge is still under investigation. Implementation of extended grids in B2.5 is foreseen in the near future [1].

5. Summary and Conclusions

In this paper, we have reported on the first application of the new SOLPS-ITER code suite to the modeling of the C-Mod divertor plasma. With its operation at high magnetic field and high density, and target shaping similar to ITER, the C-Mod divertor is particularly relevant to ITER in terms of plasma and neutral parameters.

With a fluid neutral model approximation, we can accurately reproduce upstream measurements of electron density and temperature. Asymmetries in inner - outer target ion fluxes have also been reproduced, but simulated target temperatures are too low compared with experiment.

The next steps in this work will focus on the implementation of extended grids and the inclusion of classical drifts flows and kinetic neutral particle models. Extended grids are expected to strongly improve the accuracy of the fluid neutral equation, and therefore the divertor solution for strongly shaped targets. Furthermore, the inherent uncertainty in the leakage or decay-length boundary conditions routinely applied in edge codes at radial boundaries will largely be removed.

Acknowledgement

W. Dekeyser is supported through the Monaco/ITER postdoctoral fellowship program. The views and opinions expressed herein do not necessarily reflect those of the ITER Organization. ITER is the Nuclear Facility INB-174.

[1] X. Bonnin, W. Dekeyser, R.A. Pitts *et al.*, Plasma Fusion Res. **11**, 1403102 (2016).
[2] A.S. Kukushkin, H.D. Pacher, V. Kotov *et al.*, Fusion Eng. Des. **86**, 2865 (2011).
[3] S. Wiesen, D. Reiter, V. Kotov *et al.*, J. Nucl. Mater. **463**, 480 (2015).
[4] F. Wising, D.A. Knoll, S.I. Krasheninnikov *et al.*, Contrib. Plasma Phys. **36**, 136 (1996).
[5] B. LaBombard, M.V. Umansky, R.L. Boivin *et al.*, Nucl. Fusion **40**, 2041 (2000).
[6] D.P. Stotler, R.A. Vesey, D.P. Coster *et al.*, J. Nucl. Mater.

266–**269**, 947 (1999).
[7] M.V. Umansky, D. Brunner, B. LaBombard *et al.*, Contrib. Plasma Phys. **52**, 417 (2012).
[8] D. Brunner, M.V. Umansky, B. LaBombard, *et al.*, J. Nucl. Mater. **438**, S1196 (2013).
[9] X. Bonnin, D. Coster, C.S. Pitcher *et al.*, J. Nucl. Mater. **313**–**316**, 909 (2003).
[10] N. Smick, B. LaBombard and I.H. Hutchinson, Nucl. Fusion **53**, 023001 (2013).
[11] X. Bonnin, D. Coster, R. Schneider *et al.*, J. Nucl. Mater. **337**–**339**, 301 (2005).
[12] S. Lisgo, P. Börner, C. Boswell *et al.*, J. Nucl. Mater. **337**–**339**, 139 (2005).
[13] A.S. Kukushkin, H.D. Pacher, A. Loarte *et al.*, Nucl. Fusion **49**, 075008 (2009).
[14] R. Schneider, X. Bonnin, K. Borrass *et al.*, Contrib. Plasma Phys. **46**, 3 (2006).
[15] D. Reiter, Eirene – A Monte Carlo linear transport solver, http://www.eirene.de
[16] V. Rozhansky, E. Kaveeva, P. Molchanov *et al.*, Nucl. Fusion **49**, 025007 (2009).
[17] L. Aho-Mantila, M. Wischmeier, H.W. Müller *et al.*, Nucl. Fusion **52**, 103006 (2012).
[18] F. Reimold, M. Wischmeier, M. Bernert *et al.*, J. Nucl. Mater. **463**, 128 (2015).
[19] M. Baelmans, P. Börner, W. Dekeyser *et al.*, Nucl. Fusion **51**, 083023 (2011).
[20] D. Brunner, B. LaBombard, R.M. Churchill *et al.*, Plasma Phys. Control. Fusion **55**, 095010 (2013).
[21] J.G. Watkins, R.A. Moyer, J.W. Cuthbertson *et al.*, J. Nucl. Mater. **241**–**243**, 645 (1997).
[22] J.R. Harrison, G.M. Fishpool and B.D. Dudson, J. Nucl. Mater. **463**, 757 (2015).
[23] W. Dekeyser, D. Reiter and M. Baelmans, Proc. Appl. Math. Mech. **14**, 1017 (2014).